Formation and Reactions of NH_4NO_3 during Transient and Steady-state NH_3–SCR of NO_x over H-AFX Zeolites: Spectroscopic and Theoretical Studies

Hiroe Kubota,[†] Chong Liu,*[,†] Takashi Toyao,[†,‡] Zen Maeno,[†] Masaru Ogura,[§] Naoto Nakazawa,[||] Satoshi Inagaki,[||] Yoshihiro Kubota,[||] Ken-ichi Shimizu*[,†,‡]

[†]Institute for Catalysis, Hokkaido University, N-21, W-10, Sapporo 001-0021, Japan
[‡]Elements Strategy Initiative for Catalysts and Batteries, Kyoto University, Katsura, Kyoto 615-8520, Japan
[§]Institute of Industrial Science, The University of Tokyo, 4-6-1 Komaba, Meguro-ku, Tokyo 153-8505, Japan
[||]Division of Materials Science and Chemical Engineering, Yokohama National University, 79-5 Tokiwadai, Hodogaya-ku, Yokohama 240-8501, Japan

ABSTRACT

Operando infrared (IR) spectroscopy and density functional theory (DFT) calculations were combined to investigate the selective catalytic reduction (SCR) of NO_x by NH_3 over H-AFX zeolites. The steady-state kinetics shows that SCR reactions involving NO_2 proceed much more rapidly than those of NO. Data from *in situ* IR combined with on-line mass spectrometry under transient conditions demonstrate that Brønsted acid sites (BASs) promote the reaction of NO_2 with NH_3 to form N_2, H_2O and NH_4NO_3 at low temperatures (50–150 °C). Combined with DFT results, these data suggest that NO promotes the reduction of NH_4NO_3 to NH_4NO_2, which then decomposes into N_2 and H_2O. Therefore, the accumulation of NH_4NO_3 in the zeolite is inhibited by NO. Furthermore, when NO is absent, NH_4NO_3 decomposition into N_2O and H_2O occurs only at high temperatures (> 200 °C). A comparison of H-AFX and Cu-AFX implies that Cu sites are not active for the reduction of NO_2 by NH_3, and that BASs are responsible for the NH_3–SCR reactions involving NO_2.

KEYWORDS: NH_3–SCR, AFX zeolite, kinetics study, *in situ/operando* IR, DFT calculation

1. Introduction

The selective catalytic reduction of nitrogen oxides (NO_x) by NH_3 (NH_3–SCR) is widely used to control NO_x emissions from stationary and mobile sources, including diesel vehicles.[1–4] Transition metal (Fe and Cu) cation-exchanged zeolites are promising for this purpose, and it is generally accepted that the exchanged transition metal cations are the primary catalytically active species promoting the reaction of equimolar amounts of NO and NH_3 in the presence of oxygen in so-called standard SCR.[1,2,5] The associated reaction is

$$4NH_3 + 4NO + O_2 \rightarrow 4N_2 + 6H_2O \quad (1)$$

Since the commercialization of Cu-exchanged chabazites (Cu-CHA) for use in NO_x after-treatment systems,[6,7] attention has been focused on Cu-exchanged zeolites. It has been established that the catalytic cycle during standard SCR consists of the reduction of isolated Cu(II) to Cu(I) and the subsequent reoxidation of Cu(I) to Cu(II).[1–3,5,8] Compared with Cu-CHA, the NO reduction activity of Cu-free H-CHA is negligibly low, and it has been suggested that the Brønsted acid sites (BASs) in zeolites serve as points for the exchange of Cu cations but do not themselves play a significant role in the standard SCR process.[9]

In diesel emission control systems, a diesel oxidation catalyst (DOC) located upstream of the SCR catalyst converts a portion of NO in the exhaust to NO_2, which has an important effect on the efficiency of the NH_3–SCR process.[10–21] In the case of both H-[10,11,14] and Fe-exchanged[15–17] zeolites as well as V-based catalysts,[18,19] the SCR activity is significantly enhanced at an NO_2/NO molar ratio of 1/1 (representing the so-called fast SCR reaction). The associated reaction is

$$2NH_3 + NO + NO_2 \rightarrow 2N_2 + 3H_2O \quad (2)$$

In addition, the catalytic reduction of NO_2 by NH_3 can occur without the presence of NO.[15] In the case that the N_2 selectivity of this reaction is 100%, the process is termed NO_2 SCR or slow SCR[1] and can be summarized as

$$8NH_3 + 6NO_2 \rightarrow 7N_2 + 12H_2O \quad (3)$$

The SCR activity of H-type zeolites depends significantly on the NO_2 feed. Vartuli et al. reported that the reaction rate of NO_2 SCR is several hundred times faster than that of standard SCR over H-ZSM-5 catalyst.[14] In contrast, NO_2 does not improve the NO reduction activity of Cu-zeolites.[17,22,23] He et al. recently found that the addition of NO_2 can even inhibit NO conversion at low temperatures over Cu-CHA.[24] Moreover, research data have suggested that NO_2 formed in the DOC upstream of the SCR converter can lead to the accumulation of ammonium nitrate (NH_4NO_3) in the zeolite pores, which causes catalyst deactivation [24] and the formation of the undesirable byproduct N_2O.[25]

The BASs of zeolites play a significant role in NH_3–SCR reactions involving NO_2 (that is, fast SCR and NO_2 SCR), in which Cu sites are not especially important.[10,11] In fact, because Cu sites can catalyze NO_2 decomposition to NO and O_2,[26] Cu-zeolites are not ideal model catalysts for studying the role of NO_2 in NH_3–SCR. Pioneering kinetics and theoretical studies concerning fast or NO_2 SCR utilized H-ZSM-5 zeolites,[10,13] and very little research[20] has focused on the effect of NO_2 on SCR in conjunction with small-pore H-type zeolites.[20] To the best of our knowledge, there is only limited information regarding the relative reaction rates for standard, fast and NO_2 SCR over H-type small-pore zeolites.[27]

AFX zeolite is an 8-membered ring (that is, small pore) material having both *aft* cages (0.55 × 1.35 nm) and smaller *gme* cages (0.33 × 0.74 nm).[28,29] Cu-modified AFX zeolites have recently attracted much

attention as effective catalysts for the NH_3–SCR reactions.[4,30–32] The AFX zeolites referred to as SSZ-16 have typically been synthesized using a flexible organic structure-directing agent (OSDA).[33] Recently, Kubota and co-workers developed a highly durable AFX zeolite using a bulky, non-flexible OSDA ($TEBOP^{2+}$).[28] In this study, we employed this H-type AFX (H-AFX) while performing *operando* infrared (IR) spectroscopy, kinetics and density functional theory (DFT) analyses to elucidate the role of NO_2 in NH_3–SCR under both steady-state and transient conditions. Herein, we propose mechanisms for the transformation of NO_2 to N_2 or N_2O via NH_4NO_3 over H-AFX on the basis of the experimental evidence. Subsequently, we discuss molecular-level insights into the roles of BASs and NO_2 based on the theoretical results. The mechanism uncovered herein is expected to assist in achieving rational control of NH_4NO_3 deposition and N_2O emissions during NH_3–SCR in practical systems.

2. Results and Discussion

2.1 NO_2 effect on steady-state SCR over H-AFX

To explore the effect of NO_2 on the SCR reaction rate over the H-AFX catalyst, we carried out steady-state catalytic experiments under standard SCR (NO_2/NO_x = 0), fast SCR (NO_2/NO_x = 1/2) and NO_2 SCR (NO_2/NO_x = 1) conditions, at temperatures ranging from 150 to 400 °C. An online IR spectrometer was used to determine the concentrations of the feed gas and products during these trials. It was found that the reaction rates of the fast and NO_2 SCR reactions are significantly higher than those of standard SCR, and that the NO conversions obtained from the standard SCR reaction are negligibly low under the same contact time conditions. As the NO_2/NO_x ratio was increased, the NO_x reduction rates at 200 °C increased in the following order: 0.02 mmol g^{-1} h^{-1} (NO_2/NO_x = 0), 2.89 mmol g^{-1} h^{-1} (NO_2/NO_x = 1/2), 27.36 mmol g^{-1} h^{-1} (NO_2/NO_x = 1). It is noteworthy that the NO_x reduction rates obtained using the fast SCR and NO_2 SCR processes are more than two orders of magnitude higher than that for standard SCR. These data are similar to the results in an earlier report by Stevenson et al. regarding NH_3–SCR over H-ZSM-5, in which the rate of the NO_2 SCR process is several hundred times higher than that of the standard SCR rate.[14]

Figure 1 presents Arrhenius plots with estimated apparent activation energies (E_a) for the standard, fast and NO_2 SCR reactions. The reaction rates were determined under conditions using NO_x and NH_3 that gave conversions between 20 and 55%. In the case of standard SCR, the Arrhenius plot is a straight line over the temperature range of 150–400 °C and gives an estimated E_a of 71 kJ mol^{-1}, which is larger than the literature value for standard SCR over H-ZSM-5 (56.4 kJ mol^{-1}). For fast SCR, there are two kinetic regimes with distinct apparent activation energies. The E_a is 59 kJ mol^{-1} in the high-temperature regime (275–350 °C). Unusually low apparent activation energies for fast SCR at 150–225 °C (12 kJ mol^{-1}) and NO_2 SCR (3.8 kJ mol^{-1}) suggest that the reaction is limited by diffusion. Similar temperature-dependent kinetic regimes for fast SCR over H-CHA were reported by Schneider et al.,[20] and this phenomenon was explained based on dynamic changes in active sites at certain temperatures. The data obtained for NO_2 SCR gave the lowest E_a (3.8 kJ mol^{-1}). These results indicate that the presence of NO_2 in the feed gas decreases the E_a, thereby increasing the NO_x reduction rate. With regard to product selectivity, both the standard and fast SCR selectively converted NO_x to N_2, whereas half the N was converted to N_2O during the NO_2 SCR process between 300 and 400 °C. Temperature dependence of NO_x conversion and N_2O yields is shown in Figure S1. NO_2 SCR produces relatively larger amount of N_2O due to

the undesired side reaction of Eqn. (4); N_2O yields for the NO_2 SCR reaction were around 20%, whereas N_2O yields for the standard and fast SCR reactions were below 8%. The generation of a significant amount of N_2O during NO_2 SCR over H-ZSM-5 was previously reported,[14,34] and is possibly a result of the reaction

$$2NO_2 + 2NH_3 + O_2 \rightarrow 2N_2O + 3H_2O. \qquad (4)$$

A separate experiment assessing NO oxidation by H-AFX was also performed. The rate of NO oxidation to NO_2 at 230 °C was found to be 0.12 mmol g^{-1} h^{-1}, which is close to that obtained from the standard SCR reaction (0.11 mmol g^{-1} h^{-1}). Because both fast SCR and NO_2 SCR gave higher rates than standard SCR, it is likely that NO_2 is a key intermediate in standard SCR over H-AFX, and that NO oxidation is the rate-limiting step in this process.

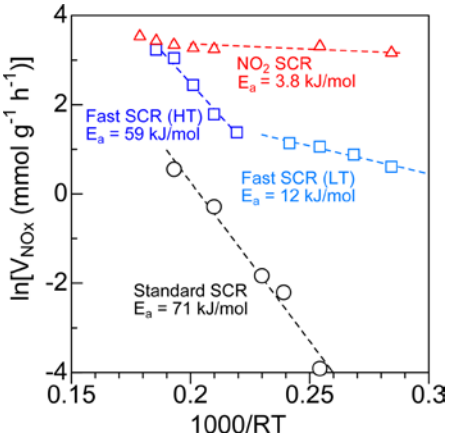

Figure 1. Arrhenius plots for standard SCR, fast SCR at high and low temperature (HT and LT) regimes, and NO_2 SCR over H-AFX zeolites.

2.2 Surface species during standard, fast and NO_2 SCR

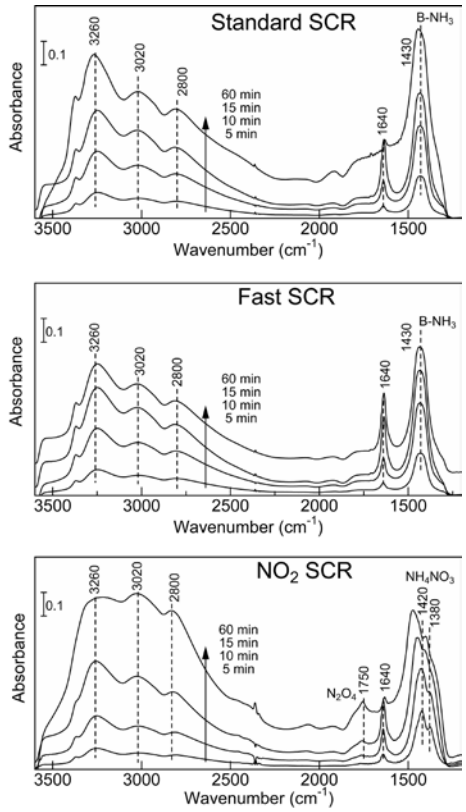

Figure 2. *In situ* IR spectra of adsorbed species on H-AFX (40 mg) during standard, fast and NO_2 SCR at 150 °C.

In situ IR spectroscopy was used to characterize the surface species generated during standard, fast and NO_2 SCR. These experiments were conducted at 150 °C using a disc of H-AFX (40 mg). As shown in Figure 2, strong IR bands due to NH_3 adsorbed on the BASs (NH_4^+ on zeolite oxygen, designated as B-NH_3) were observed at 1430, 2800, 3020 and 3260 cm^{-1} during both the standard and fast SCR reactions. In the case of standard SCR, a band most likely attributable to adsorbed NO_2 was initially observed at 1640 cm^{-1} but decreased in intensity over time. Under the steady-state standard SCR conditions (t = 60 min), B-NH_3 was evidently the dominant adsorbed species. During fast SCR, the amount of adsorbed NO_2 (associated with a peak at 1640 cm^{-1}) increased with reaction time, and both B-NH_3 and adsorbed NO_2 were present on the H-AFX at the steady state (t = 60 min). In contrast to the standard and fast SCR processes, bands at 1420 and 1380 cm^{-1} were observed during NO_2 SCR. Based on previous reports,[18,35] these bands are assigned to NH_4NO_3 accumulated on the catalyst. The bands resulting from the N–H stretching vibrations of NH_4^+ (at 2800, 3020, and 3250 cm^{-1}) in the NO_2 SCR spectra are similar to those produced during standard and fast SCR, indicating that B-NH_3 sites are also present in the catalyst under the NO_2 SCR conditions. After 60 min, a band at 1750 cm^{-1} was observed, likely due to N_2O_4 species.[36]

2.3 Transient reaction of adsorbed NH_3 with NO_x + O_2 on H-AFX and Cu-AFX

To monitor the dynamic changes in adsorbed species on the H-AFX as well as in the evolved gas products, we performed time-resolved *in situ* IR experiments at 230 °C while using mass spectrometry (MS) to evaluate the effluent gases (that is, *in situ* IR-MS or *operando* IR). In these trials, a flow type IR cell was connected to the

MS instrumentation and the H-AFX sample disc was exposed to a flow of 0.1% NH_3 in He for 10 min, followed by purging with He for 15 min. Subsequently, *in situ* IR spectra were collected as a function of time in conjunction with a flow of NO + O_2 or NO_2 + O_2 (Figure 3). After purging with He, a peak attributed to B-NH_3 sites at 1430 cm^{-1} was observed, while a band due to NH_3 adsorbed on Lewis acid sites (at approximately 1620 cm^{-1}) was not. During exposure to the NO + O_2 flow (Figure 3a), the B-NH_3 band was relatively constant for 1000 s, after which the peak intensity decreased with time. Simultaneously, an MS signal corresponding to N_2 (m/e = 28) was observed. It should be noted that the intensity of this MS peak for N_2 corresponded to the relative rate of N_2 formation. The formation of N_2 continued until the adsorbed NH_3 was completely consumed. The evident induction period of 1000 s may have been due to the blocking of active sites (Brønsted acid sites) by NH_3.[37]

When the NH_3-exposed H-AFX was treated with a flow of NO_2 + O_2 for 1000 s (Figure 3b), IR peaks assignable to NH_4NO_3 (NH_4^+ at 1420 cm^{-1} and NO_3^- at 1380 cm^{-1}) appeared. Based on reference spectra for NH_3 on BASs (B-NH_3) and NH_4NO_3, the peaks in the range of 1365-1560 cm^{-1} were deconvoluted into two components (Figure S2). The areas of each peak are plotted as functions of time in Figure 3b (right). After an induction period of 500 s, the intensity of the B-NH_3 band decreased in conjunction with N_2 formation and the accumulation of NH_4NO_3. The maximum intensity of the N_2 signal, which reflects the initial rate of N_2 formation, is higher under the NO_2 + O_2 mixture compared to the NO + O_2 trial, indicating that the reduction of NO_x by adsorbed NH_3 is faster under NO_2 + O_2. Taking into account the fact that NO_2 is produced by NO + O_2 on the BASs of zeolites,[16] the formation of N_2 over H-AFX is interpreted as the reduction of NO_2 by adsorbed NH_3 to yield N_2. As noted above, the rate of the oxidation of NO to NO_2 on H-AFX is relatively slow, such that the transient rate of N_2 formation under NO + O_2 is slower than under NO_2 + O_2.

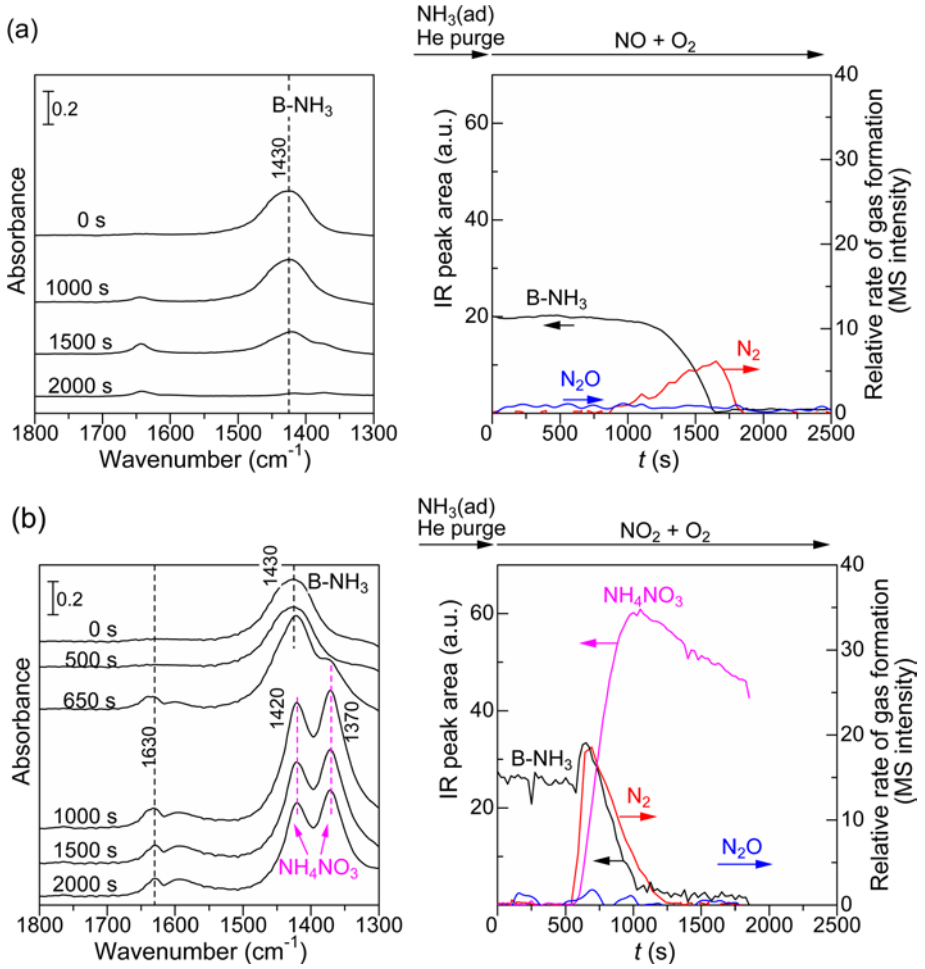

Figure 3. *In situ* IR spectra (left) of adsorbed species on H-AFX during the reaction of adsorbed NH_3 with NO_x at 230 °C (a) under 500 ppm NO + 10% O_2 and (b) under 500 ppm NO_2 + 10% O_2. The right figures show the time dependence of the IR peak area for surface species and the intensity of the MS signal for N_2.

The same experiments were then performed using NH_3-exposed Cu-AFX, and the IR-MS results under NO + O_2 and NO_2 + O_2 are shown in Figures 4a and 4b, respectively. After the He purge, the IR spectra show a peak at 1620 cm^{-1} due to NH_3 adsorbed on Cu(II) sites (designated as Cu-NH_3) together with a strong band due to the B-NH_3 (1430 cm^{-1}). When the catalyst was exposed to a flow of NO + O_2 (Figure 4a), the intensity of these bands decreased, while N_2 formation was simultaneously observed by MS analysis. Within 800 s, these NH_3 species were completely consumed to give N_2.

In contrast to the results for H-AFX (Figure 3), the transient reaction of B-NH_3 under NO_2 + O_2 over the Cu-AFX was much slower than the reaction under NO + O_2 (Figure 4). In the case of the Cu-AFX, lower rates of both B-NH_3 consumption and N_2 formation were observed under NO_2 + O_2 compared to under NO + O_2. The completion of N_2 formation under NO_2 + O_2 required more than 2000 s, while N_2 formation was complete within 800 s under NO + O_2. A comparison of the results for the SCR reactions over H-AFX and Cu-AFX in the presence of NO_2 (Figure 3b vs. Figure 4b) indicates that the Cu sites show a negative effect on the transient reaction of adsorbed NH_3 under NO_2 + O_2. This implies that the BASs serve as active sites for the reduction of NO_2 by adsorbed NH_3, while Cu sites do not play an active role in this transient reaction. Comparing

the data for H-AFX and Cu-AFX under NO + O_2 (Figure 3a vs. Figure 4a) indicates that the Cu-AFX provides a higher N_2 formation rate and more rapid B-NH_3 consumption than the H-AFX, possibly due to a higher rate of NO oxidation to NO_2 on Cu sites than on H^+ sites. The N_2 formation for the NH_3-adsorbed Cu-AFX under NO + O_2 (Figure 4b) can be explained by the following two pathways. One is the H^+-catalyzed reduction of NO_2 by adsorbed NH_3. Taking into account that Cu sites can catalyze NO_2 decomposition to O_2 and NO,[26] another possibility is the Cu-catalyzed NO_2 decomposition to give NO which is then reduced by adsorbed NH_3 over Cu sites.

Additionally, IR bands due to nitrate species on Cu^{n+} sites were observed at 1570, 1596, and 1620 cm^{-1} [38] in the spectrum obtained from the Cu-AFX under the NO_2 + O_2 mixture (Figures 4b and S3). The accumulation of these nitrates on the Cu-AFX catalyst suggests that the reaction of B-NH_3 with nitrate species on Cu sites is relatively slow. The role of such Cu nitrates in the SCR reaction is not yet fully understood, especially the question as to whether these are involved in the reaction cycle.[39,40] Nevertheless, recent time-resolved IR[40] and X-ray absorption spectroscopy (XAS)[41] studies of Cu-CHA show that the Cu nitrates are kinetically insignificant under typical low-temperature SCR conditions, indicative of their less important role in the SCR cycle.

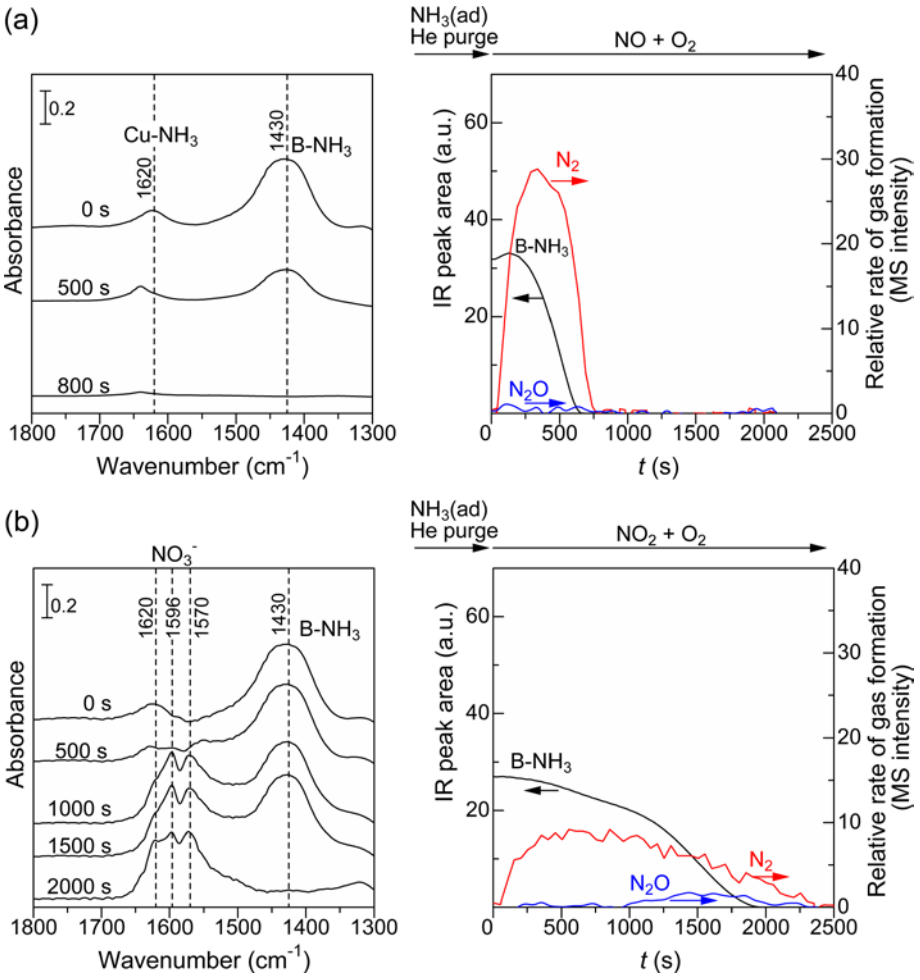

Figure 4. *In situ* IR spectra (left) of adsorbed species on Cu-AFX during the reaction of adsorbed NH_3 with NO_x at 230 °C (a) under 500 ppm NO + 10% O_2 and (b) under 500 ppm NO_2 + 10% O_2. The right figures show the

time dependence of the IR peak areas for surface species and the MS signal intensity for N_2.

2.4 Transient reaction of adsorbed NH_3 with NO_x on H-AFX

We subsequently studied the H-AFX catalyzed reaction of B-NH_3 with NO_x in the absence of O_2. Transient experiments were performed at 150 °C using NH_3-exposed H-AFX with a flow of NO + NO_2 or NO_2 (Figure 5). Under NO + NO_2, B-NH_3 was consumed by NO + NO_2 to yield N_2 after an induction period of 500 s. In contrast, the reaction under NO_2 shows a higher rate of N_2 production such that significant amounts of NH_4NO_3 were accumulated on H-AFX. The absence of NH_4NO_3 accumulation under the NO + NO_2 flow suggests that NO promoted the decomposition of NH_4NO_3[42,43] or inhibited the formation of NH_4NO_3.[35,42,43] The experimental observations suggest that NH_3 adsorbed on H^+ sites reacted with NO_2 to produce N_2 and NH_4NO_3 (Eqn. (5)). The resulting NH_4NO_3 was further able to react with NO to yield N_2, NO_2 and H_2O (Eqn. (6)).

$$2NH_{3ad} + 2NO_2 \rightarrow N_2 + NH_4NO_3 + H_2O \qquad (5)$$

$$NH_4NO_3 + NO \rightarrow N_2 + NO_2 + 2H_2O \qquad (6)$$

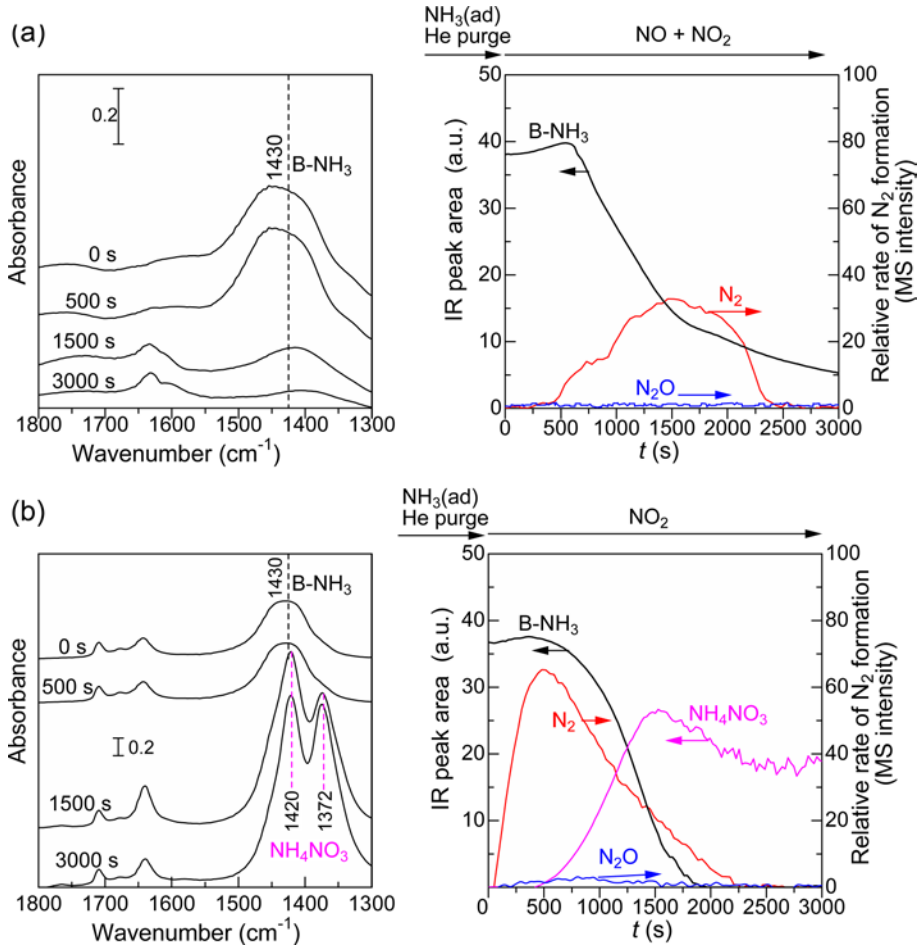

Figure 5. *In situ* IR spectra (left) of adsorbed species on H-AFX during the reaction of adsorbed NH_3 at 150 °C (a) under 250 ppm NO + 250 ppm NO_2 and (b) under 500 ppm NO_2. The right figures show the time dependence of the IR peak area for surface species and the intensity of the MS signal for N_2.

To understand the effect of temperature on reaction (5), we studied the temperature-programmed surface reaction (TPSR) of adsorbed NH_3 on H-AFX under a flow of NO_2 (Figure 6). In these trials, an IR H-AFX disc was first exposed to 0.1% NH_3 for 0.5 h at 30 °C, followed by purging with He. The catalyst was subsequently heated to 500 °C at 10 °C min^{-1} under 500 ppm NO_2. The adsorbed species and effluent gases were monitored by IR and MS, respectively. Above 50 °C, B-NH_3 consumption, N_2 formation, and NH_4NO_3 accumulation on the H-AFX were observed simultaneously. At 280 °C, NH_4NO_3 consumption and N_2O formation occurred simultaneously. These results show that reaction (5) occurs at temperature range of 50–150 °C. The reaction pathways for NH_4NO_3 conversion to N_2O and for the decomposition of NH_4NO_3 with NO to yield N_2 (Eqn. (6)) are discussed in the following section.

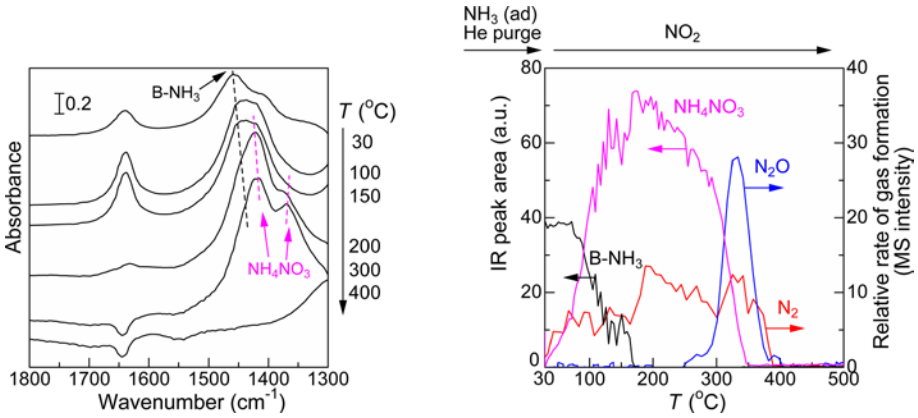

Figure 6. *In situ* IR spectra (left) acquired during the temperature-programmed surface reaction (TPSR) of adsorbed NH_3 under 500 ppm NO_2 over H-AFX, pre-exposed to 500 ppm NH_3 at 30 °C for 0.5 h. The right figure shows the time dependence of the IR peak area for surface species and the MS intensity for N_2

2.5 Conversion of NH_4NO_3 to N_2 or N_2O

To provide direct evidence for reaction (6), we carried out *in situ* IR analyses of NH_4NO_3-loaded H-AFX under a flow of NO at elevated temperatures. Based on a literature method,[23,44,45] NH_4NO_3-loaded H-AFX (NH_4NO_3 loading of 1 mmol g^{-1}) was prepared by the impregnation method, via adding 200 μL of a 0.2 M NH_4NO_3 solution dropwise to 40 mg of H-AFX, followed by drying in an oven at 80 °C for 5 h. After obtaining the background IR spectrum of the NH_4NO_3-impregnated H-AFX at 30 °C under He, the IR cell was heated (10 °C min^{-1}) under a flow of 500 ppm NO/He. Figure 7 shows the IR difference spectra of the NH_4NO_3-impregnated H-AFX at various temperatures. The negative peaks appearing at 1420, 1380, 3020 and 3260 cm^{-1} as the temperature increases indicate the consumption of adsorbed NH_4NO_3. Above 200 °C, the intensity of the negative peaks leveled off. The NO-assisted decomposition of NH_4NO_3 on SCR catalysts has also been observed in previous studies.[43,46]

In the case of the NH_4NO_3-impregnated H-AFX, the shapes of the negative peaks are close to those of the positive bands that appear when NH_3-exposed H-AFX is treated with a flow of NO_2 (Figure S4). This result suggests that the NH_4NO_3 impregnated into the H-AFX is essentially the same as the NH_4NO_3 formed by the reaction of NO_2 with NH_3. We also compared the IR spectra of physical mixtures of NH_4NO_3 and H-AFX, in

which the NH_4NO_3 particles primarily present at the external surfaces of the H-AFX. A comparison of the IR spectra (Figure S4) suggests that the physically mixed NH_4NO_3 affords different spectroscopic features to the material obtained from an NH_3 + NO_2 flow or the impregnated NH_4NO_3, indicative of the different adsorption states in these specimens. The NH_4NO_3 species generated from the reaction of NH_3 and NO_2 or impregnated from an NH_4NO_3 solution are more likely to be adsorbed on the BASs rather than at the external surfaces of the zeolite. The above comparisons demonstrate that the NH_4NO_3 sample prepared via impregnation is a better representation of the state of accumulated NH_4NO_3 during NH_3–SCR over H-AFX. Thus, we used such a sample in further TPSR trials as a model of the reaction of NH_4NO_3 inside the H-AFX zeolite. For these experiments, the amount of impregnated NH_4NO_3 (1.0 mmol g^{-1}) is less than the concentration of Al atoms in the H-AFX catalyst (2.7 mmol g^{-1}), so as to avoid over-loading of NH_4NO_3 at the external surfaces of the zeolite.

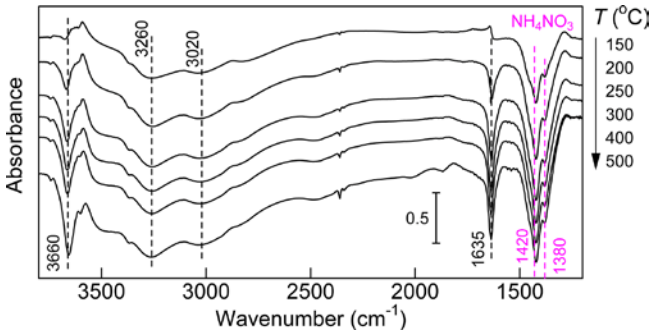

Figure 7. *In situ* IR spectra of 1 mmol g^{-1} NH_4NO_3-loaded H-AFX (40 mg) during heating from 30 to 500 °C at 10 °C min^{-1} under 500 ppm NO.

In a separate flow reactor, TPSR experiments involving NH_4NO_3(1 mmol g^{-1})-impregnated H-AFX (in powder form) were carried out under flows of various gas mixtures (Figure 8). The concentrations of both N_2 and N_2O in the effluent gas were quantified using MS. Because NO_2 was quantified by IR using a long pathlength (8 m) gas cell, the time response for NO_2 data was slower than those for the other gases. The results obtained under a flow of NO (Figure 8a) confirm the formation of N_2 and NO_2 over the temperature range of 50-200 °C. Note that the slow decay of the signal associated with the NO_2 concentration above 200 °C can be ascribed to the slower response of the IR detector compared to the MS instrument. The formation of NO_2 indicates that NH_4NO_3 is reduced by NO to yield NO_2 and ammonium nitrite (NH_4NO_2), which is consistent with the pathway proposed by Weitz et al.[43,47,48] It is also well known that NH_4NO_2 readily decomposes to N_2 and H_2O at low temperatures (< 100 °C).[47,48] Combined with the corresponding IR results in Figure 7, these data indicate that reaction (6) is actually the combination of the following two reactions.

$$NH_4NO_3 + NO \rightarrow NO_2 + NH_4NO_2 \quad (7)$$

$$NH_4NO_2 \rightarrow N_2 + 2H_2O \quad (8)$$

In the absence of NO, the decomposition of NH_4NO_3 can afford N_2O,[42,49] and the TPSR profile (Figure 8b) obtained under a He flow in the absence of NO shows N_2O formation between 200 and 350 °C with only a trace amount of N_2. This indicates that N_2O was produced via the decomposition of NH_4NO_3 in the absence of NO, as in the following reaction (Eqn. (9)).[42]

$$NH_4NO_3 \rightarrow N_2O + 2H_2O \quad (9)$$

The TPSR profile acquired under NO_2 flow (Figure 8c) shows that N_2O was the main product. This can be explained by considering that NO_2 decomposition to NO and O_2 is slow over H-AFX, such that reaction (9) proceeds more rapidly than reaction (7).

Under NH_3–SCR conditions, NH_3 co-exists in the gas mixture, and so we also studied the effect of NH_3 on the reactivity of NH_4NO_3 under NO (Figure 8d). The TPSR profile of NH_4NO_3-loaded H-AFX under a flow of an NO + NH_3 mixture shows reduced N_2 formation compared to the amount generated under NO. Additionally, N_2O formation was accelerated by the addition of NH_3. It is therefore obvious that NH_3 inhibits reaction (6) and most likely reaction (7), such that reaction (9) is accelerated. Previously, Weitz et al.[43] studied the role of BASs of zeolites in the reduction of NH_4NO_3 by NO, and reported that these sites catalyze reaction (8). Under a flow of an NO + NH_3 mixture at low temperatures, NH_3 can be readily adsorbed on the BASs of H-AFX, reducing the number of such sites available for reaction (8) and lowering the amount of N_2 formed during TPSR analyses. The TPSR experiments using NH_4NO_3-SiO_2 under NO provided no evidence for the formation of N_2 or N_2O (results not shown), indicating that the BASs are active sites for the key reactions for the formation of N_2 and N_2O (that is, reactions (7) and (9)).

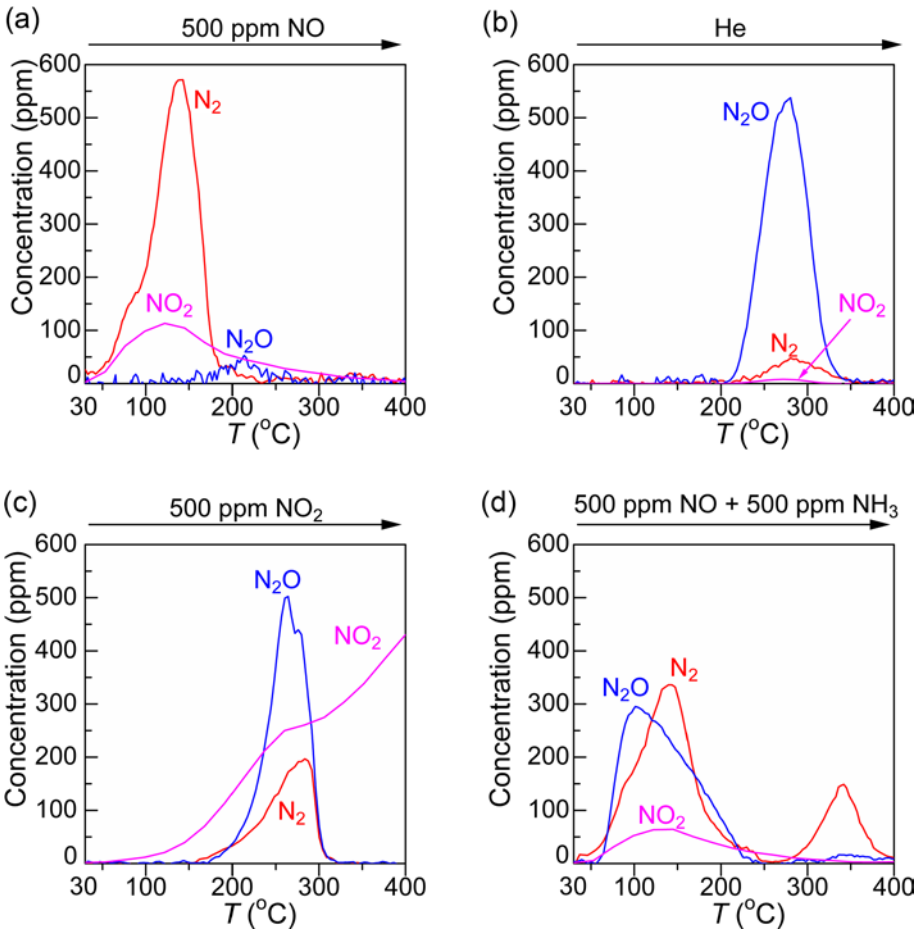

Figure 8. The TPSR profiles obtained using 1 mmol g^{-1} NH_4NO_3-loaded H-AFX (40 mg) during heating from 30 to 400 °C at 10 °C min^{-1} under (a) 500 ppm NO, (b) He, (c) 500 ppm NO_2 and (d) 500 ppm NO + 500 ppm NH_3.

2.6 DFT study on NH_4NO_3 decomposition

To provide molecular-level insights into the elementary steps of NH_4NO_3 conversion over H-AFX, we further performed DFT calculations using a 48T hexagonal unit cell (Figure S5). The formation of N_2O from NH_4NO_3 was initially investigated (Figure 9a). The adsorption of NH_4NO_3 on the protonic H-AFX zeolite was found to result in the proton transfer from the BAS to the nitrate moiety, giving HNO_3 and NH_4^+. These species in turn are stabilized by hydrogen-bonding interactions at the negative oxygen sites of the zeolite framework. The decomposition of NH_4NO_3 into N_2O proceeds via two sequential dehydration reactions. The first dehydration occurs via a proton transfer from NH_4^+ to the OH moiety of the protonated nitrate group, which produces the H_2NNO_2 intermediate with simultaneous proton back-donation to the zeolite framework oxygen (Int_H_2NNO_2). This reaction is endothermic by 84 kJ/mol with an activation energy barrier of 138 kJ/mol. In the corresponding transition state (TS1), a water molecule is already generated, and the NO_2 moiety interacts with the NH_3 fragment at an N–N distance ($d_{N–N}$) of 2.67 Å. The production of the H_2NNO_2 intermediate is accompanied by N–N bond formation ($d_{N–N}$ = 1.48 Å) and the regeneration of a BAS. The reorientation of the H_2NNO_2 intermediate (Int_H_2NNO_2(reo)) decreases the system energy by -38 kJ/mol and initiated the second dehydration reaction. With the participation of both the BAS and the water generated from the first dehydration, the conversion of H_2NNO_2 via TS2 proceeds with an activation barrier of 52 kJ/mol, and the production of N_2O significantly stabilizes the system by -91 kJ/mol. During the BAS-catalyzed decomposition of NH_4NO_3 into N_2O and H_2O, the first dehydration producing the H_2NNO_2 intermediate is the rate-determining step, with an activation barrier of 138 kJ/mol. When H-AFX is absent, the non-catalytic decomposition of NH_4NO_3 requires a much higher energy barrier of 181 kJ/mol for the first dehydration (Figure S6), indicative of the essential catalytic role of BASs during the conversion of NH_4NO_3 into N_2O.

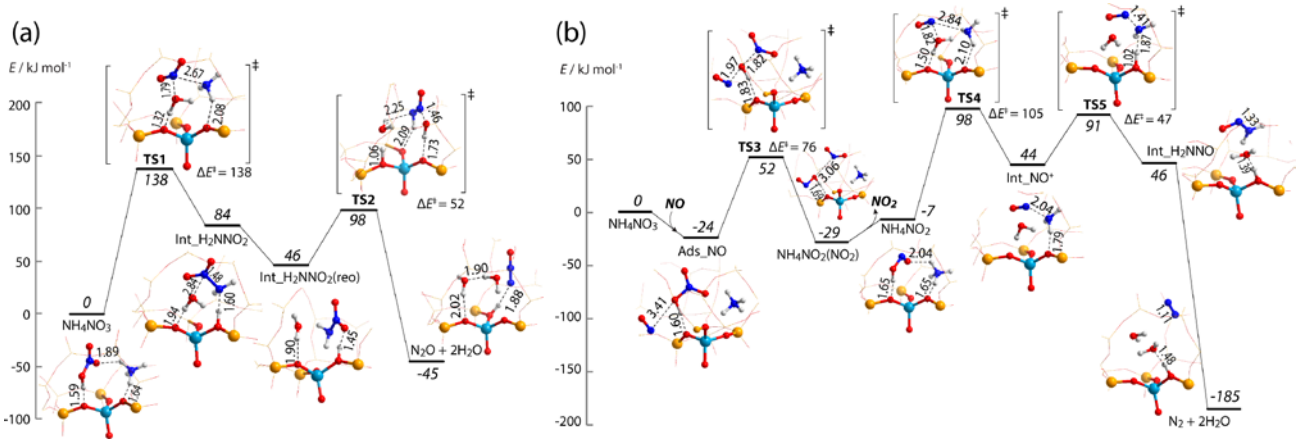

Figure 9. Energy profiles for the decomposition of NH_4NO_3 on the protonic H-AFX zeolite: (a) direct decomposition of NH_4NO_3 and (b) NO-assisted NH_4NO_3 decomposition via an NH_4NO_2 intermediate. Atomic distances are in Å.

The NO-assisted NH_4NO_3 decomposition was subsequently investigated and compared (Figure 9b). Based on our experimental evidence, it was assumed that NO first reacts with NH_4NO_3 to generate NO_2 and NH_4NO_2, which then decomposes into N_2 and H_2O. The DFT results suggest that the production of NH_4NO_2 is

realized by the hydroxyl group transfer from the protonated nitrate group (HNO_3) to the adsorbed NO, which generates nitrous acid (HNO_2) and free NO_2 ($HNO_3 + NO \rightarrow HNO_2 + NO_2$). This reaction passes through TS3 with an activation barrier of 76 kJ/mol. The release of NO_2 leads to the formation of HNO_2 and NH_4^+ stabilized at the negative oxygen sites of zeolite, which can be considered as equivalent to adsorbed NH_4NO_2 with its nitrite group protonated by the BAS. During the conversion from ammonium nitrate to nitrite, the NH_4^+ moiety is not directly involved but rather acts as a spectator. The following decomposition reaction of the NH_4NO_2 is similar to that of NH_4NO_3, although the activation barrier for the first dehydration is much lower (TS4, $\Delta E^{\ddagger}$ = 105 kJ/mol) than for NH_4NO_3 (TS1, $\Delta E^{\ddagger}$ = 138 kJ/mol). In contrast to NH_4NO_3 decomposition, in which H_2NNO_2 is produced in a single elementary step, the decomposition of NH_4NO_2 to H_2NNO occurs via a stepwise mechanism, in which NO^+ intermediate is formed (Int_NO^+ in Figure 9b). The cationic nature of this NO^+ intermediate was confirmed by Bader charge analysis (Figure S7). Compared with free gaseous NO (Q_N = +0.52 e) or adsorbed NO in a siliceous AFX framework (Q_N = +0.50 e), this NO^+ possesses a much higher positive charge on the terminal N (Q_N = +0.80 e, Int_NO^+ in Figure S7), which is similar to the case (Q_N = +0.86 e) when surrounding adsorbed NH_3 and H_2O were removed and only NO^+ was present at the negative site of $1Al^{3+}$ substituted AFX as charge-compensation cation. Such a NO^+ intermediate shows a high reactivity towards further reaction with NH_3, which requires an activation barrier of only 47 kJ/mol (TS5) to afford an H_2NNO intermediate and a Brønsted proton connected back to the zeolite framework oxygen. The decomposition of H_2NNO subsequently occurs via proton transfers,[50,51] which affords the final products of N_2 and H_2O with a strong exothermicity. The various reactions of NH_4NO_3 over H-AFX are summarized in Scheme 1.

Scheme 1. DFT-calculated reaction pathways for NH_4NO_3 decomposition under (a) non-NO-assisted and (b) NO-assisted conditions during NH_3–SCR reaction over H-AFX

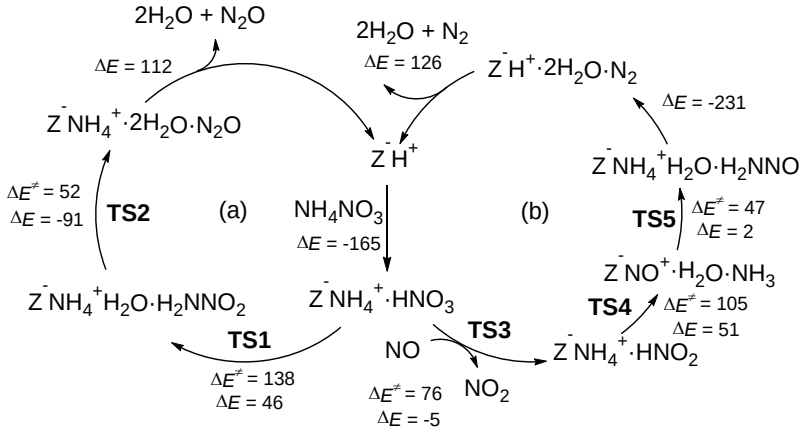

A comparison of the reaction profiles (Figure 9 and Scheme 1) indicates that direct NH_4NO_3 decomposition requires a much higher reaction energy barrier than NO-assisted NH_4NO_3 decomposition. To further assess temperature and entropy effects, we considered the Gibbs free energies of the key elementary steps (Table S1). These thermodynamic values were calculated using the results of frequency analysis. At a reaction temperature of 150 °C, the computed Gibbs free activation energies are 113 and 96 kJ/mol (TS1 and TS4) for the first dehydration reactions of NH_4NO_3 and NH_4NO_2, respectively. For the reaction of NO with

NH_4NO_3, the Gibbs free energy activation barrier to TS3 was calculated using the reference states of NH_4NO_3 and gaseous NO. The resulting value of 99 kJ/mol contains significant translational and rotational entropic contributions of free-state NO, as the adsorption process involves a strong negative entropy effect. The Gibbs free energy calculations show that the reaction of NO and NH_4NO_3 to afford NO_2 and NH_4NO_2 has a similar energy barrier (99 kJ/mol) to the further dehydration of NH_4NO_2 (96 kJ/mol). In addition, these free energy barriers are lower than that of the first dehydration reaction of NH_4NO_3 (113 kJ/mol), which is the rate-determining step in direct NH_4NO_3 decomposition. These data confirm that NO-assisted NH_4NO_3 decomposition to produce N_2 is more favorable than direct NH_4NO_3 decomposition to N_2O, which is consistent with our experimental observations.

2.7 Reaction pathways of NH_3–SCR over H-AFX zeolite via NH_4NO_3

Summarizing the above experimental and theoretical results, the reaction pathways for NH_3–SCR via NH_4NO_3 over H-AFX are shown in Scheme 2. The initial important role of the BASs is to store NH_3 by forming NH_4^+. Following this, the BASs catalytically promote the reaction of the adsorbed NH_3 with NO_2 to yield N_2, H_2O, and adsorbed NH_4NO_3 in the temperature range of 50–150 °C (Figure 6). The rate of NO reduction under the NO_2-free (standard) SCR conditions is two orders of magnitude lower than the NO_x reduction rates under fast SCR and NO_2 SCR conditions (Figure 1), possibly because NO_2 formation from BAS-catalyzed NO oxidation is too slow. Hence, the addition of NO_2 significantly enhances the NO_x reduction rate. When NO is present (in the case of fast SCR conditions), the reduction of NH_4NO_3 by NO yields gas-phase NO_2 (Figure 8a) and NH_4NO_2, which then decompose into N_2 (Figure 8a) and H_2O at low temperatures. Hence, NH_4NO_3 accumulation in the zeolite is retarded by NO (Figures 2, 5a, and 9a). NH_3 inhibits this process by blocking the BASs that otherwise serve as active sites for NH_4NO_3 reduction with NO (Figure 8d). In the absence of NO, NH_4NO_3 decomposition into N_2O and H_2O is catalyzed by BASs above 200 °C (Figures 6, 8b, and 9b). During steady-state fast SCR, the NH_4NO_3 formed on the catalyst is quickly consumed by reaction with NO, so that NH_4NO_3 does not accumulate on the catalyst (Figure 2). In the case of NO_2 SCR, the NH_4NO_3 intermediate cannot react with NO and instead decomposes into N_2O and H_2O above 200 °C. Consequently, nearly half the reduced product of steady-state NO_2 SCR is N_2O. It should be noted that NH_4NO_3 may be continuously accumulated on the catalyst below 200 °C, which makes it difficult to measure the steady-state reaction rates of the NO_2 SCR in this temperature range. In the case of the metal-exchanged SCR catalyst, Cu (or Fe) sites catalyze the oxidation of NO to NO_2, which results in higher rates of NH_4^+ consumption under NO + O_2 (Figure 4a). This pathway may contribute to the removal of NO during transient operation of the SCR system.

Scheme 2. Proposed mechanism for the NH_3–SCR reaction over H-AFX

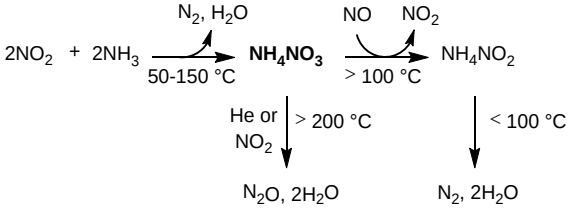

3. Conclusion

This study investigated the formation and reactions of NH_4NO_3 during the transient and steady-state NH_3–SCR of NO_x over H-AFX zeolites using *operando* IR spectroscopy, kinetics analysis and DFT calculations. Steady-state kinetics demonstrates that the SCR of NO_2 or NO/NO_2 mixture is more than two orders of magnitude faster than the SCR of NO. In the case of SCR involving NO_2 over H-AFX, BASs play an essential role by promoting the reaction of the adsorbed NH_3 with NO_2 to yield N_2, H_2O, and adsorbed NH_4NO_3 at low temperatures (50–150 °C). Transient *operando* IR and DFT studies suggest that, when NO is present, NH_4NO_3 is reduced by NO to yield NO_2 and NH_4NO_2, after which NH_4NO_2 decomposes into N_2 and H_2O. Thus, NH_4NO_3 accumulation in the zeolite is retarded by the presence of NO. In the absence of NO, the decomposition of NH_4NO_3 into N_2O and H_2O is more difficult, which only occurs at high temperatures (> 200 °C) with the assistance of BASs. A comparison of the SCR performance between H-AFX and Cu-AFX suggests that Cu sites only promote NH_3–SCR under $NO + O_2$ but show a negative effect under $NO_2 + O_2$, indicating that BASs rather than Cu sites are active for the reduction of NO_2 by adsorbed NH_3. The presented results emphasize the essential roles of BASs and NO_2 in the SCR over zeolite catalysts.

Author Information

Corresponding authors

*E-mail for K.S.:kshimizu@cat.hokudai.ac.jp.

*E-mail for C.L.:chongliu@cat.hokudai.ac.jp.

Associated Content

Supporting Information

The Supporting Information is available free of charge on the ACS Publications website at http://pubs.acs.org.

Experimental details for sample preparation, NH_3–SCR reactions, *in situ* IR and on-line MS, and temperature-programmed surface reaction (TPSR) experiments; details regarding DFT calculations; additional theoretical results.

ACKNOWLEDGEMENT

This research is one of the projects promoted by the research association of Automotive Internal Combustion Engines (AICE) and was financially supported by the Japan Ministry of Economy, Trade and Industry. Funding was also obtained from JST-CREST (JPMJCR17J3), JSPS KAKENHI (17H01341, 18K14057 and 18K14051), the MEXT project “Elements Strategy Initiative to Form Core Research Centers” and IRCCS. The authors sincerely thank the Technical Division of the Institute for Catalysis at Hokkaido University for manufacturing the experimental equipment used in this work. C.L. acknowledges the assistance of a JSPS postdoctoral fellowship (no. P19059). Part of the calculations involved in this research were performed on supercomputers at RIIT (Kyushu University) and ACCMS (Kyoto University).

References

(1) Paolucci, C.; Di Iorio, J. R.; Ribeiro, F. H.; Gounder, R.; Schneider, W. F. Catalysis Science of NOx Selective Catalytic Reduction With Ammonia Over Cu-SSZ-13 and Cu-SAPO-34. *Adv. Catal.* **2016**, *59*, 1–107. https://doi.org/10.1016/bs.acat.2016.10.002.

(2) Beale, A. M.; Gao, F.; Lezcano-Gonzalez, I.; Peden, C. H. F.; Szanyi, J. Recent Advances in Automotive Catalysis for NO_x Emission Control by Small-Pore Microporous Materials. *Chem. Soc. Rev.* **2015**, *44* (20), 7371–7405. https://doi.org/10.1039/c5cs00108k.

(3) Liu, F.; Yu, Y.; He, H. Environmentally-Benign Catalysts for the Selective Catalytic Reduction of NO_x from Diesel Engines: Structure-Activity Relationship and Reaction Mechanism Aspects. *Chem. Commun.* **2014**, *50* (62), 8445–8463. https://doi.org/10.1039/c4cc01098a.

(4) Priya, S. V.; Ohnishi, T.; Shimada, Y.; Kubota, Y.; Masuda, T.; Nakasaka, Y.; Matsukata, M.; Itabashi, K.; Okubo, T.; Sano, T.; Tsunoji, N.; Yokoi, T.; Ogura, M. A Collective Case Screening of the Zeolites Made in Japan for High Performance NH_3-SCR of NO_X. *Bull. Chem. Soc. Jpn.* **2018**, *91* (3), 355–361. https://doi.org/10.1246/bcsj.20170352.

(5) Xin, Y.; Li, Q.; Zhang, Z. Zeolitic Materials for $DeNO_x$ Selective Catalytic Reduction. *ChemCatChem* **2018**, *10* (1), 29–41. https://doi.org/10.1002/cctc.201700854.

(6) Luo, J.; Tang, Y.; Joshi, S.; Kamasamudram, K.; Currier, N.; Yezerets, A. The Impact of Ammonium Nitrate Species on Low Temperature NOx Conversion Over Cu/CHA SCR Catalyst. *SAE Int. J. Engines* **2017**, *10* (4), 1691–1696. https://doi.org/10.4271/2017-01-0953.

(7) Ottinger, N.; Xi, Y.; Keturakis, C.; Liu, Z. G. Impact of Hydrothermal Aging on the Formation and Decomposition of Ammonium Nitrate on a Cu/Zeolite SCR Catalyst. *SAE Int. J. Engines* **2017**, *10* (4), 1646–1652. https://doi.org/10.4271/2017-01-0946.

(8) Mao, Y.; Wang, Z.; Wang, H. F.; Hu, P. Understanding Catalytic Reactions over Zeolites: A Density Functional Theory Study of Selective Catalytic Reduction of NO_x by NH_3 over Cu-SAPO-34. *ACS Catal.* **2016**, *6* (11), 7882–7891. https://doi.org/10.1021/acscatal.6b01449.

(9) Bates, S. A.; Verma, A. A.; Paolucci, C.; Parekh, A. A.; Anggara, T.; Yezerets, A.; Schneider, W. F.; Miller, J. T.; Delgass, W. N.; Ribeiro, F. H. Identification of the Active Cu Site in Standard Selective Catalytic Reduction with Ammonia on Cu-SSZ-13. *J. Catal.* **2014**, *312*, 87–97. https://doi.org/10.1016/j.jcat.2014.01.004.

(10) Eng, J.; Bartholomew, C. H. Kinetic and Mechanistic Study of NO_x Reduction by NH_3 over H-Form Zeolites I. Kinetic and Mechanistic Insights into NO Reduction over H-ZSM-5. *J. Catal.* **1997**, *171* (1), 14–26. https://doi.org/10.1006/jcat.1997.1769.

(11) Eng, J.; Bartholomew, C. H. Kinetic and Mechanistic Study of NO_x Reduction by NH_3 over H-Form Zeolites II. Semi-Steady-State and In Situ FTIR Studies. *J. Catal.* **1997**, *44* (2), 27–44.

(12) Brüggemann, T. C. Theoretical Investigation of the Selective Catalytic Reduction of Nitrogen Oxides with Ammonia on Fe/H-ZSM5. *J. Phys. Chem. C* **2008**, *112* (44), 17378–17387.

(13) Brüggemann, T. C.; Keil, F. J. Theoretical Investigation of the Mechanism of the Selective Catalytic Reduction of Nitric Oxide with Ammonia in the Presence of Oxygen on H-Form Zeolites. *J. Phys.*

Chem. C **2010**, *114* (14), 6567–6587.

(14) Stevenson, S. A.; Vartuli, J. C. The Selective Catalytic Reduction of NO_2 by NH_3 over HZSM-5. *J. Catal.* **2002**, *208* (1), 100–105. https://doi.org/10.1006/jcat.2002.3542.

(15) Long, R. Q.; Yang, R. T. Temperature-Programmed Desorption/Surface Reaction (TPD/TPSR) Study of Fe-Exchanged ZSM-5 for Selective Catalytic Reduction of Nitric Oxide by Ammonia. *J. Catal.* **2001**, *198* (1), 20–28. https://doi.org/10.1006/jcat.2000.3118.

(16) Long, R. Q.; Yang, R. T. Reaction Mechanism of Selective Catalytic Reduction of NO with NH_3 over Fe-ZSM-5 Catalyst. *J. Catal.* **2002**, *207* (2), 224–231. https://doi.org/10.1006/jcat.2002.3528.

(17) Colombo, M.; Nova, I.; Tronconi, E. A Comparative Study of the NH_3-SCR Reactions over a Cu-Zeolite and a Fe-Zeolite Catalyst. *Catal. Today* **2010**, *151* (3–4), 223–230. https://doi.org/10.1016/j.cattod.2010.01.010.

(18) Tronconi, E.; Nova, I.; Ciardelli, C.; Chatterjee, D.; Weibel, M. Redox Features in the Catalytic Mechanism of the "Standard" and "Fast" NH_3-SCR of NO_x over a V-Based Catalyst Investigated by Dynamic Methods. *J. Catal.* **2007**, *245* (1), 1–10. https://doi.org/10.1016/j.jcat.2006.09.012.

(19) Koebel, M.; Madia, G.; Elsener, M. Selective Catalytic Reduction of NO and NO_2 at Low Temperatures. *Catal. Today* **2002**, *73* (3–4), 239–247. https://doi.org/10.1016/S0920-5861(02)00006-8.

(20) Li, S.; Zheng, Y.; Gao, F.; Szanyi, J.; Schneider, W. F. Experimental and Computational Interrogation of Fast SCR Mechanism and Active Sites on H-Form SSZ-13. *ACS Catal.* **2017**, *7* (8), 5087–5096. https://doi.org/10.1021/acscatal.7b01319.

(21) Li, J.; Li, S. New Insight into Selective Catalytic Reduction of Nitrogen Oxides by Ammonia over H-Form Zeolites: A Theoretical Study. *Phys. Chem. Chem. Phys.* **2007**, *9* (25), 3304–3311. https://doi.org/10.1039/b700161d.

(22) Grossale, A.; Nova, I.; Tronconi, E.; Chatterjee, D.; Weibel, M. The Chemistry of the NO/NO_2-NH_3 "Fast" SCR Reaction over Fe-ZSM5 Investigated by Transient Reaction Analysis. *J. Catal.* **2008**, *256* (2), 312–322. https://doi.org/10.1016/j.jcat.2008.03.027.

(23) Xie, L.; Liu, F.; Liu, K.; Shi, X.; He, H. Inhibitory Effect of NO_2 on the Selective Catalytic Reduction of NO_x with NH_3 over One-Pot-Synthesized Cu-SSZ-13 Catalyst. *Catal. Sci. Technol.* **2014**, *4* (4), 1104–1110. https://doi.org/10.1039/c3cy00924f.

(24) Shan, Y.; Shi, X.; He, G.; Liu, K.; Yan, Z.; Yu, Y.; He, H. Effects of NO_2 Addition on the NH_3-SCR over Small-Pore Cu-SSZ-13 Zeolites with Varying Cu Loadings. *J. Phys. Chem. C* **2018**, *122* (45), 25948–25953. https://doi.org/10.1021/acs.jpcc.8b05930.

(25) Szanyi, J.; Kollár, M.; Peden, C. H. F.; Wang, Y.; Washton, N. M.; Gao, F. Effects of Si/Al Ratio on Cu/SSZ-13 NH_3-SCR Catalysts: Implications for the Active Cu Species and the Roles of Brønsted Acidity. *J. Catal.* **2015**, *331*, 25–38. https://doi.org/10.1016/j.jcat.2015.08.004.

(26) Morpurgo, S. The Mechanism of NO and N_2O Decomposition Catalyzed by Short-Distance Cu(I) Pairs in Cu-ZSM-5: A DFT Study on the Possible Role of NO and NO_2 in the $[Cu–O–Cu]^{2+}$ Active Site Reduction. *J. Catal.* **2018**, *366* (2), 189–201. https://doi.org/10.1016/j.jcat.2018.08.006.

(27) Iwasaki, M.; Shinjoh, H. A Comparative Study of “Standard”, “Fast” and “NO_2” SCR Reactions over Fe/Zeolite Catalyst. *Appl. Catal. A Gen.* **2010**, *390* (1–2), 71–77. https://doi.org/10.1016/j.apcata.2010.09.034.

(28) Nakazawa, N.; Inagaki, S.; Kubota, Y. Novel Technique to Synthesize AFX-Type Zeolite Using a Bulky and Rigid Diquaternary Ammonium Cation. *Adv. Porous Mater.* **2016**, *4* (3), 219–229. https://doi.org/10.1166/apm.2016.1114.

(29) Davis, T. M.; Liu, A. T.; Lew, C. M.; Xie, D.; Benin, A. I.; Elomari, S.; Zones, S. I.; Deem, M. W. Computationally Guided Synthesis of SSZ-52: A Zeolite for Engine Exhaust Clean-Up. *Chem. Mater.* **2016**, *28* (3), 708–711. https://doi.org/10.1021/acs.chemmater.5b04578.

(30) Martín, N.; Paris, C.; Vennestrøm, P. N. R.; Thøgersen, J. R.; Moliner, M.; Corma, A. Cage-Based Small-Pore Catalysts for NH_3-SCR Prepared by Combining Bulky Organic Structure Directing Agents with Modified Zeolites as Reagents. *Appl. Catal. B Environ.* **2017**, *217*, 125–136. https://doi.org/10.1016/j.apcatb.2017.05.082.

(31) Chokkalingam, A.; Chaikittisilp, W.; Iyoki, K.; Keoh, S. H.; Yanaba, Y.; Yoshikawa, T.; Kusamoto, T.; Okubo, T.; Wakihara, T. Ultrafast Synthesis of AFX-Type Zeolite with Enhanced Activity in the Selective Catalytic Reduction of NOx and Hydrothermal Stability. *RSC Adv.* **2019**, *9* (29), 16790–16796. https://doi.org/10.1039/c9ra02787d.

(32) Shibata, G.; Eijima, W.; Koiwai, R.; Shimizu, K.; Nakasaka, Y.; Kobashi, Y.; Kubota, Y.; Ogura, M.; Kusaka, J. NH3-SCR by Monolithic Cu-ZSM-5 and Cu-AFX Catalysts: Kinetic Modeling and Engine Bench Tests. *Catal. Today* **2019**, *332* (May 2018), 59–63. https://doi.org/10.1016/j.cattod.2018.06.023.

(33) Fickel, D. W.; D’Addio, E.; Lauterbach, J. A.; Lobo, R. F. The Ammonia Selective Catalytic Reduction Activity of Copper-Exchanged Small-Pore Zeolites. *Appl. Catal. B Environ.* **2011**, *102* (3–4), 441–448. https://doi.org/10.1016/j.apcatb.2010.12.022.

(34) Wallin, M.; Karlsson, C. J.; Skoglundh, M.; Palmqvist, A. Selective Catalytic Reduction of NO_x with NH_3 over Zeolite H-ZSM-5: Influence of Transient Ammonia Supply. *J. Catal.* **2003**, *218* (2), 354–364. https://doi.org/10.1016/S0021-9517(03)00148-9.

(35) Ciardelli, C.; Nova, I.; Tronconi, E.; Chatterjee, D.; Bandl-Konrad, B.; Weibel, M.; Krutzsch, B. Reactivity of NO/NO_2-NH_3 SCR System for Diesel Exhaust Aftertreatment: Identification of the Reaction Network as a Function of Temperature and NO_2 Feed Content. *Appl. Catal. B Environ.* **2007**, *70* (1–4), 80–90. https://doi.org/10.1016/j.apcatb.2005.10.041.

(36) Penkova, A.; Hadjiivanov, K.; Mihaylov, M.; Daturi, M.; Saussey, J.; Lavalley, J. C. FTIR Spectroscopic Study of Low Temperature NO Adsorption and NO + O_2 Coadsorption on H-ZSM-5. *Langmuir* **2004**, *20* (13), 5425–5431. https://doi.org/10.1021/la0496643.

(37) Grossale, A.; Nova, I.; Tronconi, E. Ammonia Blocking of the “Fast SCR” Reactivity over a Commercial Fe-Zeolite Catalyst for Diesel Exhaust Aftertreatment. *J. Catal.* **2009**, *265* (2), 141–147. https://doi.org/10.1016/j.jcat.2009.04.014.

(38) Ruggeri, M. P.; Nova, I.; Tronconi, E.; Pihl, J. A.; Toops, T. J.; Partridge, W. P. In-Situ DRIFTS Measurements for the Mechanistic Study of NO Oxidation over a Commercial Cu-CHA Catalyst. *Appl.*

Catal. B Environ. **2015**, *166–167* (2), 181–192. https://doi.org/10.1016/j.apcatb.2014.10.076.

(39) Janssens, T. V. W.; Falsig, H.; Lundegaard, L. F.; Vennestrøm, P. N. R.; Rasmussen, S. B.; Moses, P. G.; Giordanino, F.; Borfecchia, E.; Lomachenko, K. A.; Lamberti, C.; Bordiga, S.; Godiksen, A.; Mossin, S.; Beato, P. A Consistent Reaction Scheme for the Selective Catalytic Reduction of Nitrogen Oxides with Ammonia. *ACS Catal.* **2015**, *5* (5), 2832–2845. https://doi.org/10.1021/cs501673g.

(40) Zhang, Y.; Peng, Y.; Li, K.; Liu, S.; Chen, J.; Li, J.; Gao, F.; Peden, C. H. F. Using Transient FTIR Spectroscopy to Probe Active Sites and Reaction Intermediates for Selective Catalytic Reduction of NO on Cu/SSZ-13 Catalysts. *ACS Catal.* **2019**, 6137–6145. https://doi.org/10.1021/acscatal.9b00759.

(41) Marberger, A.; Petrov, A. W.; Steiger, P.; Elsener, M.; Kröcher, O.; Nachtegaal, M.; Ferri, D. Time-Resolved Copper Speciation during Selective Catalytic Reduction of NO on Cu-SSZ-13. *Nat. Catal.* **2018**, *1* (3), 221–227. https://doi.org/10.1038/s41929-018-0032-6.

(42) Shan, Y.; Shi, X.; He, G.; Liu, K.; Yan, Z.; Yu, Y.; He, H. Effects of NO_2 Addition on the NH_3-SCR over Small-Pore Cu-SSZ-13 Zeolites with Varying Cu Loadings. *J. Phys. Chem. C* **2018**, *122* (45), 25948–25953. https://doi.org/10.1021/acs.jpcc.8b05930.

(43) Savara, A.; Li, M. J.; Sachtler, W. M. H.; Weitz, E. Catalytic Reduction of NH_4NO_3 by NO: Effects of Solid Acids and Implications for Low Temperature $DeNO_x$ Processes. *Appl. Catal. B Environ.* **2008**, *81* (3–4), 251–257. https://doi.org/10.1016/j.apcatb.2007.12.008.

(44) Ruggeri, M. P.; Luo, J.; Nova, I.; Tronconi, E.; Kamasamudram, K.; Yezerets, A. Novel Method of Ammonium Nitrate Quantification in SCR Catalysts. *Catal. Today* **2018**, *307* (April 2017), 48–54. https://doi.org/10.1016/j.cattod.2017.04.016.

(45) Pereira, M. V. L.; Berthout, D.; Petitto, C.; Delahay, G.; Raux, S.; Rousseau, S. Ammonium Nitrate Temperature-Programmed Decomposition on Fe–Zeolite Catalysts: Effect of Deposition Method. *ChemCatChem* **2017**, *9* (12), 2339–2343. https://doi.org/10.1002/cctc.201700147.

(46) Selleri, T.; Gramigni, F.; Nova, I.; Tronconi, E. NO Oxidation on Fe- and Cu-Zeolites Mixed with BaO/Al2O3: Free Oxidation Regime and Relevance for the NH3-SCR Chemistry at Low Temperature. *Appl. Catal. B Environ.* **2018**, *225*, 324–331. https://doi.org/10.1016/j.apcatb.2017.11.068.

(47) Li, M.; Henao, J.; Yeom, Y.; Weitz, E.; Sachtler, W. M. H. Low Activation Energy Pathway for the Catalyzed Reduction of Nitrogen Oxides to N_2 by Ammonia. *Catal. Lett.* **2004**, *98* (1), 5–9. https://doi.org/10.1007/s10562-004-6441-y.

(48) Li, M.; Yeom, Y.; Weitz, E.; Sachtler, W. M. H. An Acid Catalyzed Step in the Catalytic Reduction of NO_x to N_2. *Catal. Lett.* **2006**, *112* (3–4), 129–132. https://doi.org/10.1007/s10562-006-0191-y.

(49) Chen, H. Y.; Wei, Z.; Kollar, M.; Gao, F.; Wang, Y.; Szanyi, J.; Peden, C. H. F. A Comparative Study of N_2O Formation during the Selective Catalytic Reduction of NOx with NH_3 on Zeolite Supported Cu Catalysts. *J. Catal.* **2015**, *329*, 490–498. https://doi.org/10.1016/j.jcat.2015.06.016.

(50) Sun, D.; Schneider, W. F.; Adams, J. B.; Sengupta, D. Molecular Origins of Selectivity in the Reduction of NO_x by NH_3. *J. Phys. Chem. A* **2004**, *108* (43), 9365–9374. https://doi.org/10.1021/jp049079a.

(51) Paolucci, C.; Verma, A. A.; Bates, S. A.; Kispersky, V. F.; Miller, J. T.; Gounder, R.; Delgass, W. N.;

Ribeiro, F. H.; Schneider, W. F. Isolation of the Copper Redox Steps in the Standard Selective Catalytic Reduction on Cu-SSZ-13. *Angew. Chem. Int. Ed.* **2014**, *53* (44), 11828–11833. https://doi.org/10.1002/anie.201407030.

TOC